Numerical simulation of pore pressure changes in Champlain clays - Sainte-Marthe study case

Amirhossein Shafaei, François Duhaime, Vahid Marefat
Department of Construction Engineering – École de technologie supérieure (ÉTS), Montreal, Quebec, Canada

ABSTRACT
Pore pressure changes due to loading, soil moisture change, and climate play a key role regarding instability and volume changes for Champlain clays. In this study, the pore pressure record for the Sainte-Marthe test site was replicated using a numerical model based on the finite element method and the Biot (1941) consolidation theory. Based on the shallow depth of the water table, the soil domain was assumed to be fully saturated. The changes in upper boundary conditions (mechanical load due to soil moisture changes and pore pressure changes due to water table fluctuations) were applied using the van der Kamp and Gale (1983) theory. The soil properties for the model were based on the pore pressure response to barometric pressure changes and laboratory permeability tests. The model was calibrated using pore pressure records and historical climate data. The final calibrated model based on the routing of a constant percentage of infiltration as runoff can replicate the historical data reasonably well.

RÉSUMÉ
Les changements de pression interstitielle dus au chargement, au changement de teneur en eau du sol et au climat jouent un rôle clé en ce qui concerne l'instabilité et les changements de volume pour les argiles Champlain. Dans cette étude, des mesures de pression interstitielle pour le site expérimental de Sainte-Marthe ont été reproduites à l'aide d'un modèle numérique basé sur la méthode des éléments finis et la théorie de la consolidation de Biot (1941). Sur la base de la faible profondeur de la nappe phréatique, il a été supposé que le sol était complètement saturé. Les changements dans les conditions aux limites supérieures (charge mécanique due aux changements de l'humidité du sol et fluctuations de l'élévation de la nappe phréatique) ont été appliqués au modèle à l'aide de la théorie de van der Kamp et Gale. (1983). Les propriétés du sol pour le modèle ont été obtenues sur la base de la réponse de la pression interstitielle aux changements de pression barométrique et d'essais de perméabilité au laboratoire. Le modèle a été calibré en utilisant des mesures de pression interstitielle et des données climatiques historiques. Le modèle final calibré suppose que le ruissellement représente une proportion constante de l'infiltration. Ce modèle reproduit raisonnablement bien les données historiques.

1 INTRODUCTION

Sensitive Champlain clay deposits occupy a large portion of the Saint-Lawrence River valley. Modelling pore pressure changes in Champlain clays is an important problem in geotechnical engineering. These pore pressure changes influence both the clay shear strength and volume change properties. The relationship between pore pressure changes and settlements has been documented in the literature. For instance, Silvestri (2000) observed some annual settlement cycles with an amplitude of up to 50 mm and pore pressure cycles with an amplitude of up to 35 kPa on the Island of Montreal.

Several approaches can be used to model pore pressure changes in soil. Biot (1941) developed an approach based on the Terzaghi (1925) consolidation theory and effective stress principle that can model the soil behaviour under varying stress and hydraulic conditions. The Biot theory was later simplified by van der Kamp and Gale (1983) to model one dimensional pore pressure variations due to loading. This model has been used to analyze the pore pressure variations in soil and rock for various applications involving an external loading. A large number of these studies focused on the analysis of soil moisture balance (e.g., van der Kamp and Maathuis 1991; van der Kamp and Schmidt 1997; Barr et al. 2000; van der Kamp and Schmidt 2017). Other studies applied this model for different purposes. For example, Chen et al. (2015) investigated the relationship between groundwater level fluctuations and stress changes using GPS data and observed precipitation time series before an earthquake in Taiwan. Chang and Yeh (2016) studied solute transport in a saturated porous medium with variable hydraulic conductivity which deforms in response to stress changes. Pacheco and Fallico (2015) simulated the response of a confined aquifer to river stage variations and mechanical loading.

A few studies have looked specifically at the modelling of pore pressures in low-permeability soils (aquitards). The low permeability of aquitards isolate them from the pore pressure changes at their top or bottom surface (Barr et al. 2000). Pore pressure changes in thick aquitards, in most cases, only reflect the changes of mechanical loading on the formation (van der Kamp and Schmidt 1997). Anochikwa et al. (2012), using this characteristic of aquitards, simulated the pore pressure variation induced by surface loading and groundwater level fluctuation utilizing the van der Kamp and Gale (1983) theory. They applied a new approach based on a superposition technique that made it possible to replicate separately the pore pressure response to mechanical loading or water table fluctuations in a stiff clay layer below a surficial layer of gravel and sand.

Pore pressure changes in the subsurface induce displacements in the soil skeleton. By measuring in situ displacements using an extensometer, Murdoch et al.

(2015) developed a viable technique to characterize average load changes that occur over vast areas of soil.

The purpose of this investigation is to develop a FEM model for estimating the effects of hydrological and climate times series on pore pressure changes in Champlain clays. This model will first be used to replicate the pore pressure changes that were measured in the intact clay layer of the Sainte-Marthe test site in response to soil moisture changes and groundwater movements in the upper fractured clay layer. As this model will later be used to study the influence of climate change on the geotechnical engineering of Champlain clay deposits, it should also take into account the stress-strain deformation of the soil. The approach that was applied in this paper is mainly based on the works of Biot (1941) and van der Kamp and Gale (1983).

2 STUDY SITE DESCRIPTION

The study site is located in the province of Quebec, in Canada. It is located approximately 45 km west of the city of Montreal between the Ottawa and St. Lawrence Rivers, in the municipality of Sainte-Marthe (45°24'29" N, 74°18'07" W). The study area is located between Highway 40 to the north, Road 325 to the west, Road 340 to the south and Road 201 to the east.

The geology of this study site is similar to other areas of the St. Lawrence lowlands. Most the region comprises flat lands under cultivation. The stratigraphy of the region indicates the existence of two main clay layers: a fractured clay layer and an intact clay layer. The stiff, fractured and brownish clay can be found up to a depth of 5 m. Under this layer, there is an intact clay layer with a thickness of around 10 m. The intact clay is highly sensitive (sensitivity up to 200) at depths ranging from 6 to 10 m. The bedrock depth is around 21 m. The clay layer and the bedrock are separated by a silty layer (Marefat et al. 2017).

The Sainte-Marthe monitoring site was established in October 2016. This study site includes three 114 mm boreholes. Two of them reach a depth of 22 m in the bedrock, while the other well was drilled to a depth of 12 m in the clay layer.

The drilling was done using a wash boring method and flush-joint straight casings. Four standpipe piezometers and four vibrating wire piezometers (VWP) were installed in these three boreholes (Marefat et al. 2017). The VWP can measure pore pressures in the range of 0-350 kPa with an accuracy of ± 1 mm. Two monitoring wells with an intake zone at a depth of 21 m were installed in boreholes F1 and F2. In boreholes F1 and F3, two VWP were installed at depths of 6.1 m and 12.2 m. Two 21 mm standpipes were installed at the same depths in borehole F2. A transducer with a full-scale range of 100 kPa was also installed in a standpipe which was completed below the water table in borehole F2. This transducer is recording the groundwater movement in the upper fractured clay layer (Figure 2).

The first purpose of this study site was to examine the different parameters of the fully-grouted installation method for piezometers (Marefat et al. 2018). The most reliable measurements were selected for the present study. The pore pressure record in the intact clay layer was obtained at a depth of 12.1 m in borehole F1 (Piezometer F1B), while the groundwater level variation in the fractured clay was acquired by the F2 transducer.

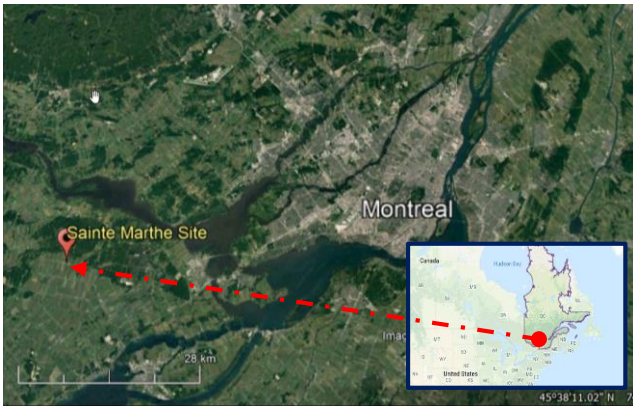

Figure 1. Sainte-Marthe (Google Maps)

3 THEORETICAL BACKGROUND

In this section, the theoretical background of the Biot (1941) consolidation theory and van der Kamp and Gale (1983) equation is presented.

3.1 Biot-Darcy Poroelasticity model

The Biot (1941) theory of consolidation defines the relationship between the stress and strain tensors of the soil. For transient water flow in a porous medium that obeys Darcy's law, the Biot (1941) differential equations of consolidation are as follows:

$$G\nabla^2 u + \frac{G}{1-2v}\frac{\partial \epsilon}{\partial x} - \alpha\frac{\partial p}{\partial x} = 0 \quad [1]$$

$$G\nabla^2 v + \frac{G}{1-2v}\frac{\partial \epsilon}{\partial y} - \alpha\frac{\partial p}{\partial y} = 0 \quad [2]$$

$$G\nabla^2 w + \frac{G}{1-2v}\frac{\partial \epsilon}{\partial z} - \alpha\frac{\partial p}{\partial z} = 0 \quad [3]$$

$$k_h\nabla^2 \mathrm{p} = \alpha\frac{\partial \epsilon}{\partial t} + \frac{1}{Q}\frac{\partial p}{\partial t} \quad [4]$$

where $\nabla^2 = \partial^2/\partial x^2 + \partial^2/\partial y^2 + \partial^2/\partial z^2$, k_h is the coefficient of permeability of the soil (hydraulic conductivity), ϵ represents the volume increase of the soil per unit initial volume (volumetric strain), p is the increment of water pressure, u, v, w are the components of displacement respectively in x, y, z directions, G is the shear modulus, v is Poisson's ratio, α defines the ratio of the volume of water squeezed-out of the soil to the volume change of the soil in drained condition. The coefficient $1/Q$ is the amount of

water that can be added to the soil under pressure while the volume of the soil is maintained constant.

3.2 van der Kamp and Gale (1983)

Van der Kamp introduced a one-dimensional model for estimating the pore pressure changes in response to surface loading and transient flow in the saturated porous medium based on the Biot (1941) theory:

$$\frac{\partial p}{\partial t} = (D\frac{\partial^2 p}{\partial z^2} + \gamma\frac{\partial \sigma}{\partial t}) \quad [5]$$

where p is pore pressure change, γ is the elastic pore pressure coefficient (loading efficiency or tidal efficiency), σ is mechanical load and D is the hydraulic diffusivity which is equal to the ratio of hydraulic conductivity to specific storage. It is worth mentioning that the barometric and earth tidal effects were removed in this equation. So, in order to use this equation, the in situ pressure data should be corrected for both effects.

According to this theory, if an aquifer that is infinite in horizontal extent is subjected to vertical stresses over a large area, the resulting horizontal displacement will be small and can be neglected. As a result, the deformation of the porous skeleton can be assumed to be only vertical.

4 METHODOLOGY

The pore pressure variation in the Sainte-Marthe clay deposit in response to hydrological time series can be estimated using the Biot equations of poroelasticity. Some simplifications and assumptions based on the van der Kamp and Gale (1983) theory were used to specify the boundary condition. The model only considers transient flow in the saturated intact clay layer.

4.1 Conceptual model

The conceptual model in this study is a one-dimensional soil column. The soil column height is 16 m from the top of the intact clay layer to the bottom where it reaches to bedrock. The unconfined aquifer (unsaturated layer) is excluded from the model domain. As a result, the conceptual model is fully saturated and the water table fluctuation and soil moisture changes (net water balance) will be applied to the top of the domain as a boundary condition. The domain material is assumed to be isotropic with uniform hydraulic conductivity and elastic properties.

4.2 Boundary conditions:

There are two active boundary conditions at the top of the domain. These boundary conditions are water level movements and stress changes due to soil moisture variation (Anochikwa et al. 2012). The groundwater table fluctuation measured by the transducer defines the active hydraulic boundary condition at the top.

The net water balance in the fractured layer specifies the top stress boundary condition, the term $\partial\sigma/\partial t$ in equation 5. These changes are obtained by calculating the weight of the available soil moisture in the upper layer with the following equation:

$$\sigma(0,t) = \rho_f g(P_R - ET - R) \quad [6]$$

where σ is total stress, t is time, ρ_f is the fluid density, g is an acceleration of gravity, P_R is precipitation, ET is evapotranspiration and R is runoff height. All these parameters should be cumulative in order to estimate the net water flux to the domain.

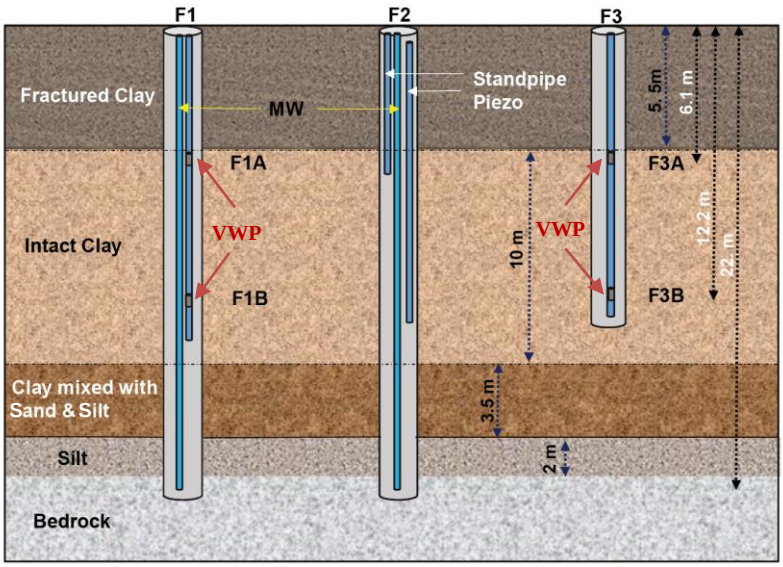

Figure 2. Cross-sectional profile of the study site (MW: monitoring wells)

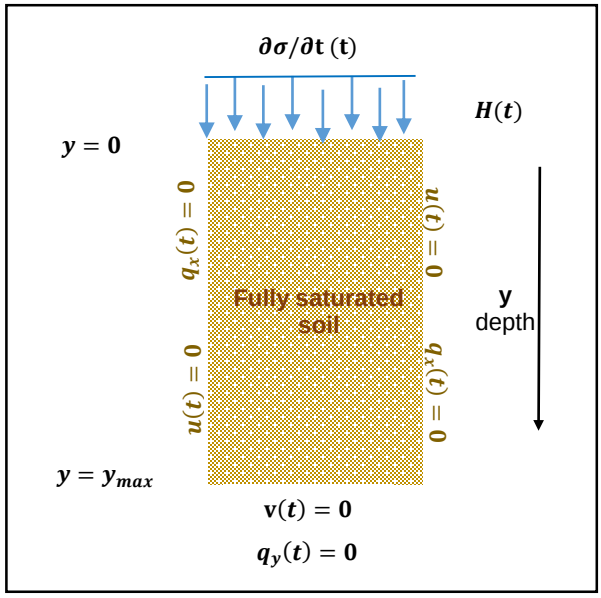

Figure 3. Boundary condition in 1D conceptual model (where *H* is the hydraulic head, *σ* is total stress, *u* and *v* are respectively horizontal and vertical displacements, q_x and q_y are water fluxes in x and y directions)

For this study, the daily precipitation data were obtained from an experimental weather station located approximately 2.2 km away from the boreholes. While there was no actual evapotranspiration data available for the region, the required data was estimated using ETo Calculator software (Raes 2012). This application uses the FAO Penman-Monteith equation for assessment of evapotranspiration (Allen et al. 1998). This method was selected as it explicitly takes into consideration both physiological and aerodynamic parameters. Furthermore, it can closely approximate the actual evapotranspiration of grass, the main ground cover around the study site. This approach was examined in a study by Armstrong et al. (2008) for Canadian prairie landscape. The results showed a reasonable agreement with observed data.

The required meteorological data for the FAO Penman-Monteith method are daily maximum and minimum temperatures, daily dew point temperature, daily wind speed and daily solar radiation. All these parameters except solar radiation were obtained from the Sainte-Marthe weather station. For solar radiation, the open access satellite-based data provided by NASA POWER project was applied (Stackhouse 2018).

The runoff volume during the first step was assumed to be zero. The average runoff height during the simulation was estimated by applying different runoff scenarios that will be described later in the paper. The best runoff scenario was chosen by comparing the observed and simulated pressure data. The boundary conditions and domain are illustrated in Figure 3.

The hydraulic head boundary condition at the top of the domain is the measured water table fluctuation. This data was obtained from the shallow transducer in the fractured layer. The observed pressures were corrected for barometric effect using the multiple regression method as described in Marefat et al. (2015).

The boundary conditions on left and right sides of the domain were assumed to be impervious and laterally-fixed. The bottom boundary condition is fixed with no water flow. The simulation period is six months from December 2016 to May 2017.

4.3 Finite Element Model

COMSOL Multiphysics was used in this study to solve the differential equations. COMSOL Multiphysics can solve an extensive range of problems using the finite element method (Comsol 2017). COMSOL was chosen because of its capability for coupling different physics, solving and coupling partial differential equations, and programmability. In this study, the Biot poroelasticity feature of this application was used. The poroelasticity feature uses the matrix forms of the Biot equation to solve for the pressure and displacements in the soil. To simulate pore flow, the Darcy law interface uses the following equation:

$$\rho_f S \frac{\partial H}{\partial t} - \nabla.\left[\rho_f k_h \nabla H\right] = -\rho_f \alpha \frac{\partial \varepsilon}{\partial t} \quad [7]$$

where *S* is the poroelastic storage coefficient estimated based on the Young modulus (*E*) and Poisson ratio (*v*) and *H* is the hydraulic head (m). This equation is similar to equation 4. The static equilibrium equation for the poroelastic material is as follows:

$$-\nabla.\sigma = \rho g \quad [8]$$

In this equation, *σ* defines the stress tensor, *ρ* is the soil density (total mass/total volume), and *g* is gravitational acceleration. For a 2D model under isotropic and plane strain conditions, the stress tensor in equation 8 can be expressed in terms of the deformation tensor (ε_{xx}, ε_{yy}, ε_{xy}):

$$\begin{bmatrix}\sigma_{xx}\\ \sigma_{yy}\\ \sigma_{xy}\end{bmatrix} = \frac{E}{(1+v)(1-2v)}\begin{bmatrix}1-v & v & 0\\ v & 1-v & 0\\ 0 & 0 & 1-2v\end{bmatrix}\begin{bmatrix}\varepsilon_{xx}\\ \varepsilon_{yy}\\ \varepsilon_{xy}\end{bmatrix} - \begin{bmatrix}\alpha p & 0 & 0\\ 0 & \alpha p & 0\\ 0 & 0 & \alpha p\end{bmatrix} \quad [9]$$

The strain tensor can in return be defined using the displacement components. Equation 9 is another form of equations 1-3. When applying the boundary conditions mentioned previously, the COMSOL poroelasticity interface becomes in effect a one-dimensional model. This way, the model can be used to apply the van der Kamp and

Gale (1983) theory and to simulate pore pressure changes in the soil due to surficial stresses.

4.4 Intact Clay properties

The k_h value provided by falling-head laboratory tests on intact clay specimens was 1.08×10^{-9} m/s (Marefat et al. 2017). The barometric pressure response of the aquitard allowed *E* to be estimated at 50 MPa based on the van der Kamp and Gale (1983) method. With this method, *E* is calculated based on the drained constrained modulus (*EC*) by assuming a Poisson's ratio (*v*) of 1/3. The sequential steps of the simulation are illustrated in Figure 4.

5 RESULT AND DISCUSSION

Figure 5 compares the hydraulic head time series that were measured using piezometer F1B with the hydraulic head time series that were simulated at the same depth without runoff. The comparison shows a reasonable agreement between the time series with respect to the general trend and magnitude. The best-fit parameters R squared (RSQ), mean squared error (MSE), root-mean-square error (RMSE) for the simulation without runoff are summarized in Table 1. This agreement is stronger during the first two months of the simulation period. For the rest of the period, the difference between the graph lines increases. This seems to be due to the absence of runoff.

Table 1. Best-fit parameters for the model without runoff (R-squared values, root mean square error, mean squared error in hydraulic head simulations)

Parameter	Value
RSQ	0.87
RMSE (m)	0.04
MSE (m^2)	0.36

Considering the average temperature graph, it can be seen that during the period when the pore pressure graphs became more separated, the study site experienced relatively warmer days with temperatures above 0°C. Infiltration and runoff estimation in cold regions during winter is complex. In these areas, the rate of runoff is affected by factors such as freeze-thaw cycles, soil texture, precipitation form, wind speed, soil moisture content, and temperature. For instance, precipitations in the winter months mostly occurs as snow. Consequently, the runoff rate is less significant. Another possible explanation for hydraulic head differences is a relative increase in the frequency of heavy precipitation events (Figure 7). Heavy precipitation can be expected to result in a higher runoff rate. The increased gap between model results and measured data can also be related to evapotranspiration. There might be substantial differences between actual and estimated reference crop evapotranspiration. The times series of the cumulative infiltration rate ($\sum P_R$-ET), total precipitation, and evapotranspiration rate are presented respectively in Figures 6-8.

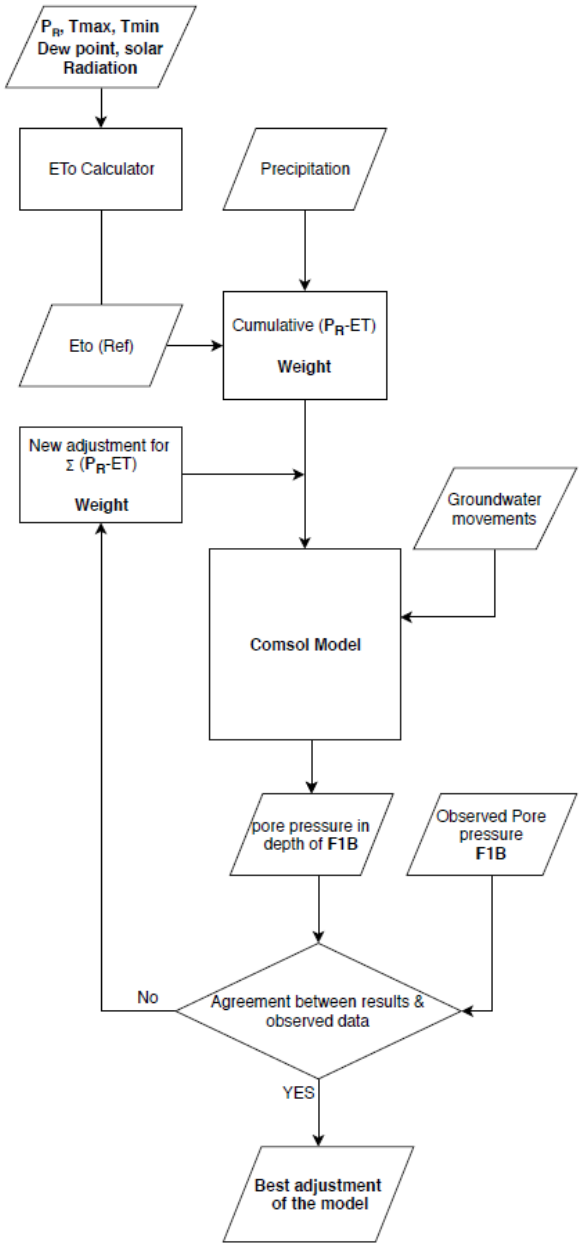

Figure 4. Simulation steps

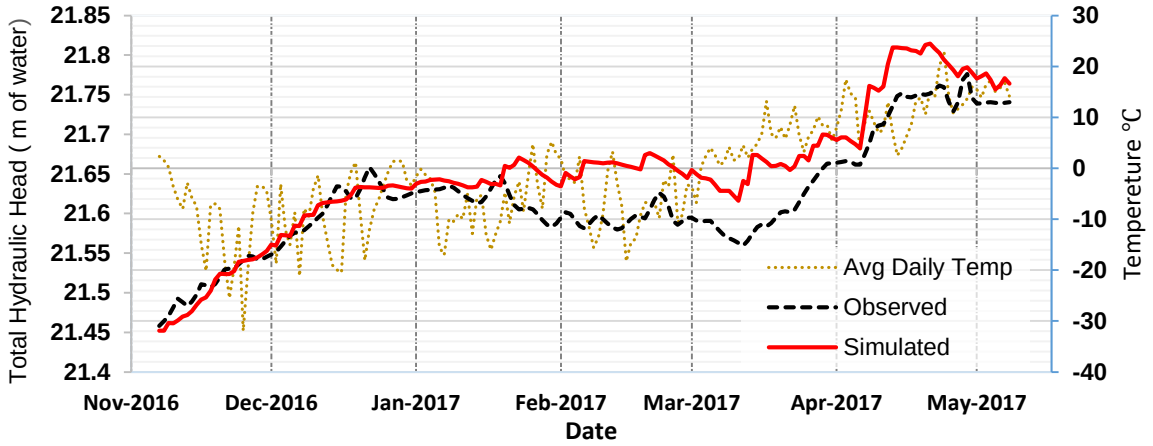

Figure 5. Time series of the simulated and observed pore pressure response in the intact layer of the study site and average daily temperature (not considering the runoff)

Considering all the above information, the infiltration rate was decreased. For this purpose, an adjustment was applied to the P_R-ET time series. A best fit was then obtained between the simulated and measured data based on the RSQ, MSE, RMSE parameters (Tables 2). Figure 9 illustrates the best adjustment of P_R-ET. In this simulation, a 24% reduction of infiltration rate was applied to the model. The results show a relative improvement in the best-fit parameters.

Table 2. Best-fit parameters for the model with runoff (24 % reduction of infiltration rate)

Parameter	Value
RSQ	0.89
RMSE(m)	0.03
MSE(m^2)	0.12

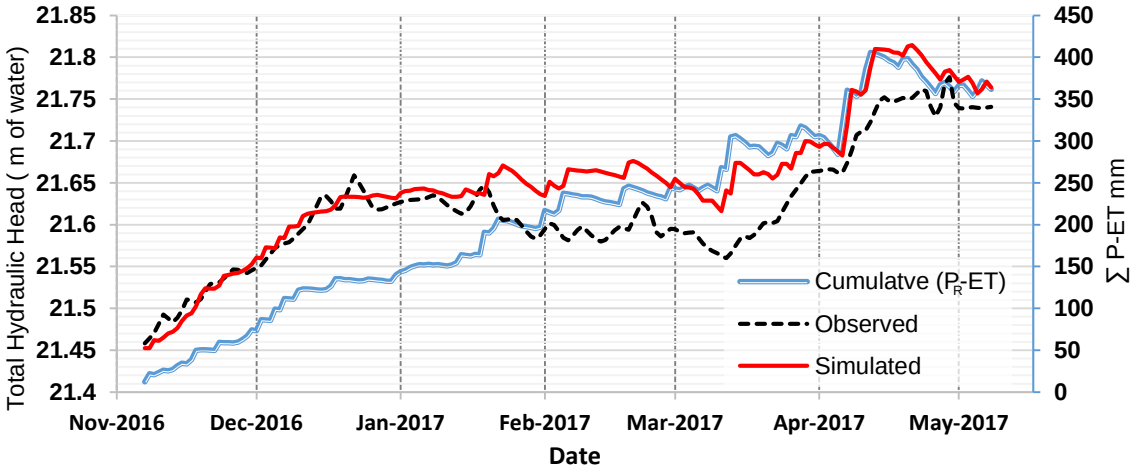

Figure 6. Time series of the simulated and observed pore pressure response in the intact layer of the study site and cumulative infiltration ($(\sum P_R$-ET)

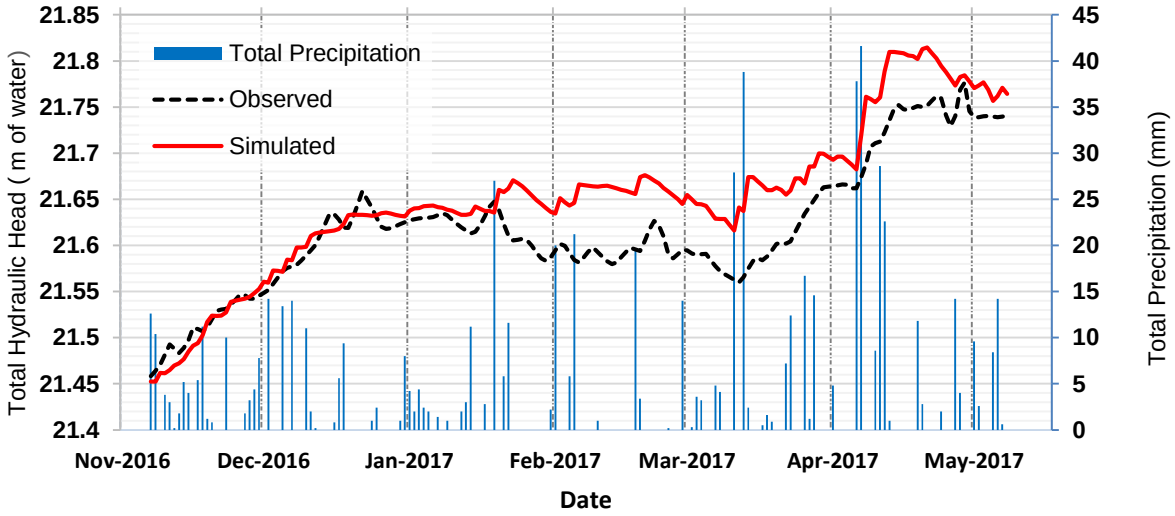

Figure 7. Time series of the simulated and observed pore pressure response in the intact layer of the study site and total precipitation.

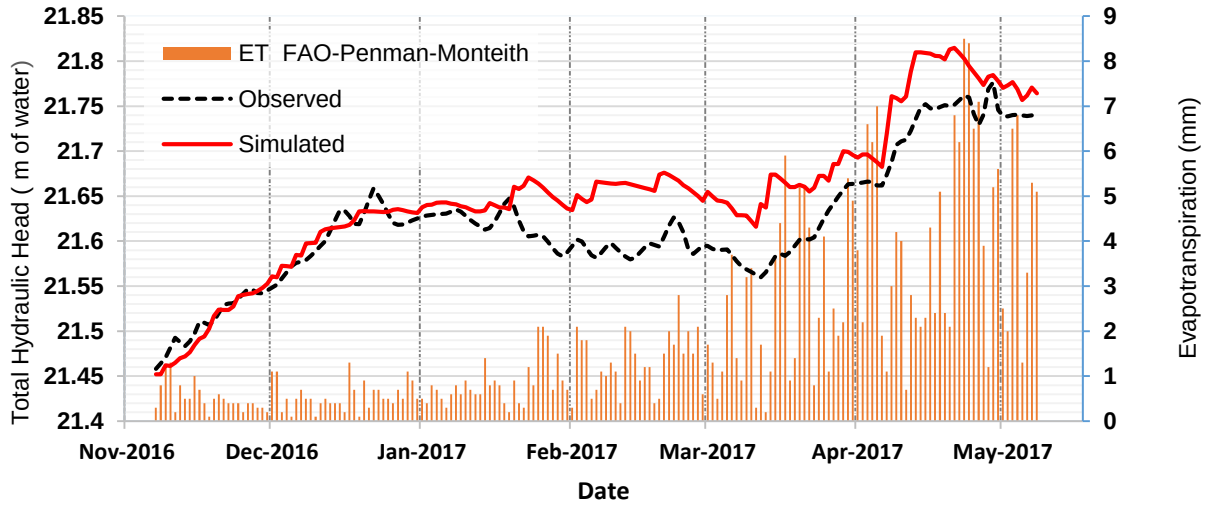

Figure 8. Time series of the simulated and observed pore pressure response in the intact layer of the study site and estimated evapotranspiration.

6 CONCLUSION

The present work investigates the effects of groundwater movements and soil moisture fluctuation on pore pressure changes in soil. A one-dimensional conceptual model was examined using the finite element approach. The results indicated a reasonable agreement between the simulated and observed pore pressure responses. However, there are still certain deficiencies that need to be addressed in future works. For instance, more accurate estimations of the runoff and evapotranspiration are needed. The simulation also needs to be performed for an extended period and for other study sites, such as the Lachenaie sites (Duhaime et al. 2013).

ACKNOWLEDGMENTS

The authors would like to acknowledge the funding of NSERC for this project.

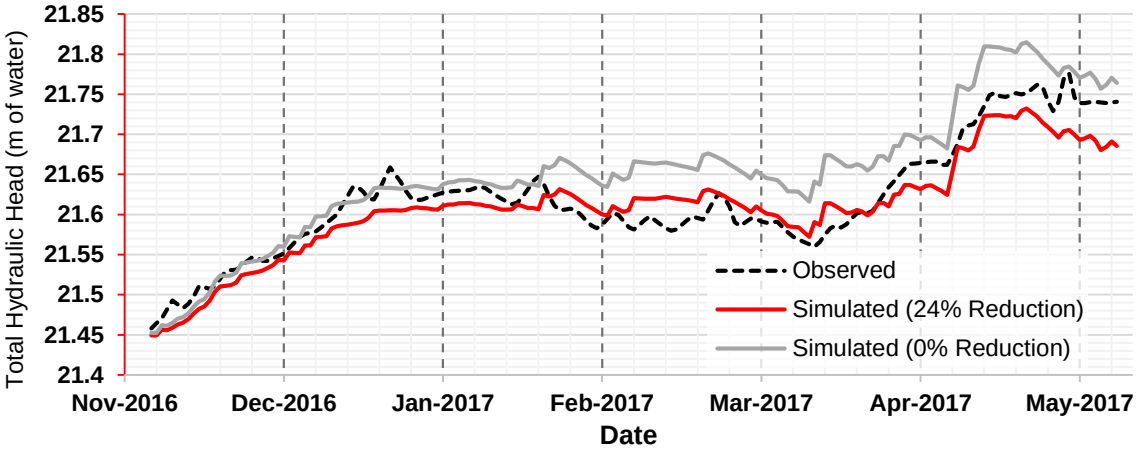

Figure 9. Time series of the simulated and observed pore pressure response in the intact layer of the study site for corrected and uncorrected infiltration rate (24% reduction of infiltration rate as a runoff).

7 REFERENCES

Allen, R., Pereira, L., Raes, D., and Smith, M. 1998. Crop evapotranspiration-Guidelines for computing crop water requirements-FAO Irrigation and drainage paper 56. *Fao, Rome* 300.9. D05109.

Anochikwa, C.I., van der Kamp, G., and Barbour, S.L. 2012. Interpreting pore-water pressure changes induced by water table fluctuations and mechanical loading due to soil moisture changes, *Canadian Geotechnical Journal*, 49: 357–366.

Armstrong, R.N., Pomeroy, J.W., and Martz, L.W. 2008. Evaluation of three evaporation estimation methods in a Canadian prairie landscape, *Hydrological Processes*, 22: 2801–2815.

Biot, M.A. 1941. General theory of three-dimensional consolidation. *Journal of Applied Physics*, 12(2): 155-164.

Chang, C.-M., and Yeh, H.-D. 2016. Investigation of flow and solute transport at the field scale through heterogeneous deformable porous media, *Journal of Hydrology*, 540: 142–147.

Chen, C.H., Tang, C.C., and Cheng, K.C. 2015. Groundwater-strain coupling before the 1999 Mw 7.6 Taiwan Chi-Chi earthquake, *Journal of Hydrology*, 524: 378–384.

COMSOL. 2017. COMSOL Multiphysics 5.3 *Reference Manual.* : 1480.

Duhaime, F.F., Benabdallah, E.M., and Chapuis, R.P. 2013. The Lachenaie clay deposit : some geochemical and geotechnical properties in relation to the salt-leaching process, *Canadian Geotechnical Journal*, 325: 311–325.

Marefat, V., Duhaime, F., and Chapuis, R.P. 2015. Pore pressure response to barometric pressure change in Champlain clay: Prediction of the clay elastic properties. *Engineering Geology*, 198: 16–29.

Marefat, V., Duhaime, F., Chapuis, R.P., and Le Borgne, V. 2017. Fully grouted piezometers in a soft Champlain clay deposit Part I: Piezometer installation, *Geotechnical News*, 35(3): 35–38.

Marefat, V., Duhaime, F., Chapuis, R.P., and Le Borgne, V. 2018. Performance of fully grouted piezometers under transient flow conditions: field study and numerical results. *Geotechnical Testing Journal*, In press.

Murdoch, L.C., Freeman, C.E., Germanovich, L.N., Thrash, C., and Dewolf, S. 2015. Using in situ vertical displacements to characterize changes in moisture load. *Water Resources Research*, 51(8): 5998–6016.

Pacheco, F.A.L., and Fallico, C. 2015. Hydraulic head response of a confined aquifer influenced by river stage fluctuations and mechanical loading, *Journal of Hydrology*, 531: 716–727.

Raes, D. 2012. The ETo Calculator. *Reference Manual Version 3.2*, FAO, Rome.

Silvestri, V. 2000. Performance of shallow foundations on clay deposits in Montréal Island, *Canadian Geotechnical Journal*, 37: 218-237.

Stackhouse, P. 2018. Prediction Of Worldwide Energy Resources. *[online]. Available from https://power.larc.nasa.gov/.*

Terzaghi, K. 1925. Erdbaumechanik auf bodenphysikalischer grundlage. *Deuticke, Leipzig, Allemagne.*

van der Kamp, G., and Gale, J.E. 1983. Theory of earth tide and barometric effects in porous formations with compressible grains, *Water Resources Research,* 19(2): 538–544.

van der Kamp, G., and Maathuis, H. 1991. Annual fluctuations of groundwater levels as a result of loading by surface moisture. *Elsevier*, 127(1–4): 137–152.

van der Kamp, G., and Schmidt, R. 1997. Monitoring of total soil moisture on a scale of hectares using groundwater piezometers. *Geophysical Research Letters*, 24(6): 719–722.

van der Kamp, G., and Schmidt, R. 2017. Review: Moisture loading—the hidden information in groundwater observation well records. *Hydrogeology Journal,* 25(8): 2225–2233.